



OPEN

First theoretical framework for highly efficient photovoltaic parameters by structural modification with benzothiophene-incorporated acceptors in dithiophene based chromophores

Muhammad Khalid^{1,2}✉, Rameez Ahmed^{1,2}, Iqra shafiq^{1,2}, Muhammad Arshad³, Muhammad Adnan Asghar⁴, Khurram Shahzad Munawar⁵, Muhammad Imran⁶ & Ataualpa A. C. Braga⁷

Now a days, researchers are constantly doing efforts to upgrade the performance of solar based devices with the aim of increasing the role of photovoltaic materials in modern hi-tech optoelectronic applications. Realizing the recent energy conditions across the globe, research is diverted from fullerene to non-fullerene electron acceptor moieties in this era, considering their remarkable contribution in organic solar cells (OSCs). Therefore, we designed seven novel non-fullerene fused ring electron acceptor chromophores (MD2–MD8) from DOC2C6-2F by structural tailoring with different acceptors at end-capped units. DFT study was performed at B3LYP functional to discover the opto-electronic characteristics of the newly tailored chromophores. Various analysis such as frontier molecular orbitals (FMOs), transition density matrix (TDM), density of states (DOS), binding energy (E_b), reorganization energy, open circuit voltage (V_{oc}) was carried out to comprehend the photovoltaic response of MD2–MD8. Decrease in band gaps (1.940–1.571 eV) with wider absorption spectrum (725.690–939.844 nm in chloroform) along with greater charge transfer rate from HOMO towards LUMO were examined in derivatives as compared to MR1 ($E_{gap} = 1.976$ eV, $\lambda_{max} = 738.221$ nm) except MD7. Further, in all derivatives, smaller values of E_b (0.252–0.279 eV) were examined than that of reference (0.296 eV). These lower binding energy values of MD2–MD8 indicated the higher rate of excitation dissociation with lager charger transfer rate than MR1, which further supported by DOS and TDM analyses. Additionally, least reorganization energy in the aforesaid compounds for hole with electron was also inspected. Moreover, V_{oc} a good photovoltaic response was noted for all studied compounds which indicated that these compounds are suitable to synthesize OSCs in future.

¹Institute of Chemistry, Khwaja Fareed University of Engineering & Information Technology, Rahim Yar Khan 64200, Pakistan. ²Centre for Theoretical and Computational Research, Khwaja Fareed University of Engineering & Information Technology, Rahim Yar Khan 64200, Pakistan. ³Department of Chemical Engineering, College of Engineering, King Khalid University, Abha, Saudi Arabia. ⁴Division of Science and Technology, Department of Chemistry, University of Education, Lahore, Pakistan. ⁵Department of Chemistry, University of Mianwali, Mianwali 42200, Pakistan. ⁶Department of Chemistry, Faculty of Science, King Khalid University, P.O. Box 9004, Abha 61413, Saudi Arabia. ⁷Departamento de Química Fundamental, Instituto de Química, Universidade de São Paulo, Av. Prof. Lineu Prestes, 748, São Paulo 05508-000, Brazil. ✉email: muhammad.khalid@kfueit.edu.pk; khalid@iq.usp.br

The technologies of OSCs have progressed in terms of architecture, processing techniques and the semiconductor materials^{1,2}. The solar cells having a promising future as a sustainable and clean replacement of fossil fuel are organic solar cells (OSCs). Due to profound advantages in manufacturing, low weight, flexibility and less expensive this photovoltaic technology has been the attention of industrial and academic community for decades³. In current scenario, the most promising approach of converting sunlight into electrical energy is through solar cells by utilization of photoelectric effect. Formerly, silicon is considered as the efficient semiconducting materials in the solar cells owing to their higher power conversion efficiency (PCE), heat constancy and ease in access. In these days, utilization of silicon in silicon based solar cells has restricted because of certain factors like high cost, brittleness and fixed energy levels⁴. Recently bulk heterojunction (BHJ)⁵ OSCs have emerged as attractive candidates for global green energy sources due to their exceptional characteristics like flexibility, semitransparency, tunable energy levels, economic viability and potential commercial applications⁶. The OSCs have a blend of donor and acceptor molecules which link directly with each other through a backbone. OSCs bearing fullerene acceptors hold appealing assets including improved PCE, higher charge mobility⁷. In spite of these advantages, there have been found certain limitations associated with fullerene acceptors that limit their use⁸. To overcome such shortcomings of fullerene derivatives, non-fullerene acceptors (NFAs)⁹ materials with acceptor-donor-acceptor (A-D-A) backbone has given a great deal of attention¹⁰. The A-D-A diversity is of peculiar interest due to their unique properties like wide and efficient absorption bands and adjustable energy levels¹¹. A-D-A combination comprises of central donor core unit which attached with two sideways electron deficient end capped acceptors through chemical bond. Narrowing the HOMO-LUMO band gap has proved the most effective strategy to enhance PCE and photovoltaic properties of non-fullerene based OSCs¹². This can be brought successfully by choosing appropriate electron donor and withdrawing parts¹³.

Two imperative classes of non-fullerene acceptors have come under study recently such as Perylene diimide (PDI)^{14,15} and fused ring electron acceptors (FREAs)¹⁶. PCEs up to 9% have been reported in OSCs with PDI non fullerene acceptor. On the other hand, OSCs retaining non-covalently fused ring electron acceptors (NC-FREAs)¹⁷ configuration have fascinating properties because of their easy structural modulation^{18,19}, strong optical absorption and enhanced PCE up to 14%²⁰. Among FREAs, the most successful and widely discussed non fullerene acceptors type is ITIC²¹ with ladder type indacenodithienothiophene as a central core and with A-D-A type architecture enabling BHJ layer to enhance charge mobility. In comparison to traditional fullerene-based acceptor, ITIC types OSCs retain PCE up to 13%²². NFAs comparatively possess superior photovoltaic properties than their fullerene counterparts, that includes higher optical absorption, promising light capturing ability and tunable energy levels^{23,24}. It is commonly observed that changing the molecular properties such as light absorbing capability, crystallinity, light absorption and energy levels by structural tailoring can effectively enhance the device performance^{25,26}.

Considering the attractive qualities of fused ring non-fullerene acceptors based OSCs, seven new A-D-A type NC-FREAs (**MD2–MD8**) from parent **DOC2C6-2F** were designed. End capped acceptor modifications has been brought about in reference chromophore and their impact on the electronic and optical behavior of newly designed chromophores are studied. It is anticipated that these newly designed derivatives will play a vital part in the development of high efficacy OSCs cell materials.

Results and discussion

Aim behind the current study is to explore the photovoltaic response of NFAs type organic compounds. For this, **DOC2C6-2F**²⁷ is selected to be used as a parent molecule comprised of central ladder-like 1,4-bis((2-ethylhexyl)peroxy)benzene core unit linked with donor (D) moiety along with two terminal electron capturing acceptor (A) components. In order to overcome the steric hinderance and computational cost caused by long alkyl chains in **DOC2C6-2F**, $C_8H_{17}O$ substituted on the donor unit is replaced with methyl ($-CH_3$) group as shown in Fig. 1. After this minute structural tailoring, the synthesized parent chromophore having A-D-A configuration is renamed as “**DOC2C6-2F**” to “**MR1**” reported as reference chromophore retaining the same A-D-A configuration.

We changed the terminal acceptors of **DOC2C6-2F** with various well known end capped acceptors just to explore and boost the electronic properties of OSCs. **MD2–MD8** molecules having A-D-A configuration as shown in Fig. 2 and Fig. S1. The optimized structures of the **MR1** and its derivative **MD2–MD8** are depicted in Fig. 3.

Frontier molecular orbital (FMO) analysis. FMO approach is believed to be an influential approach for determining the electronic characteristics of OSCs²⁸. The HOMO and LUMO are regarded as valence and conduction bands according to the valance band theory. The energy difference between HOMO and LUMO has been elucidated as the band gap (E_g)^{29–32}. Efficiency reasonably depends upon the E_g as low energy band gap concludes large photovoltaic response of a compound and vice versa³³. Computed energies and their E_g for designed chromophores are presented in Table 1.

In **MR1**, 1.976 eV E_g is noted having -5.176 and -3.200 eV HOMO and LUMO energies. Interestingly, a decrease in E_g has been noted for the designed chromophores (**MD2–MD6** and **MD8**) except **MD7** in which the E_g is larger than the reference compound (**MR1**). The energies for HOMO are noticed to be -5.158 , -5.217 , -5.180 , -5.161 , -5.210 , -5.125 and -5.116 eV for **MD2–MD8**, while for LUMO are -3.200 , -3.366 , -3.646 , -3.438 , -3.382 , -3.582 , -3.137 and -3.176 eV and the E_g between them is calculated as 1.792 , 1.571 , 1.742 , 1.779 , 1.628 , 1.988 and 1.940 eV, respectively (Table 1). In **MD2**, a decline in E_g (1.792 eV) is found due to the introduction of thiophene ring and replacement of fluoro ($-F$) with chloro ($-Cl$) groups at the terminal acceptor moieties³⁴. Another reason is the presence of thiophene ring as a result of which conjugation gets enhanced and E_g is observed to be reduced. The smallest E_g (1.571 eV) is noted for **MD3** among all the designed compounds

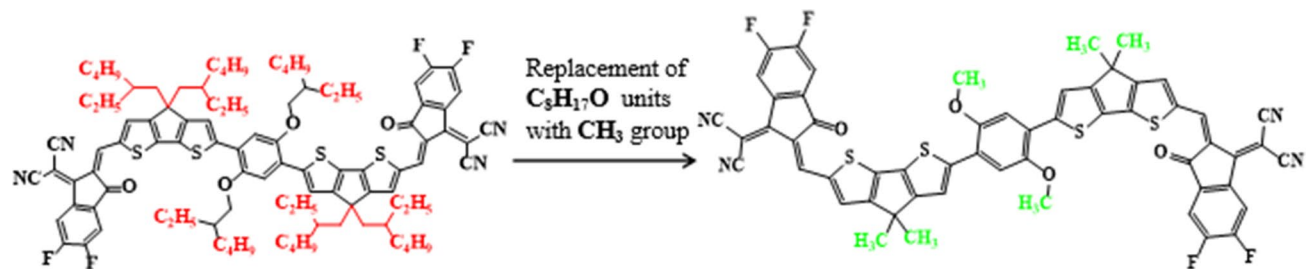


Figure 1. Modification of DOC2C6-2F into MR1 via substitution of -CH₃ group.

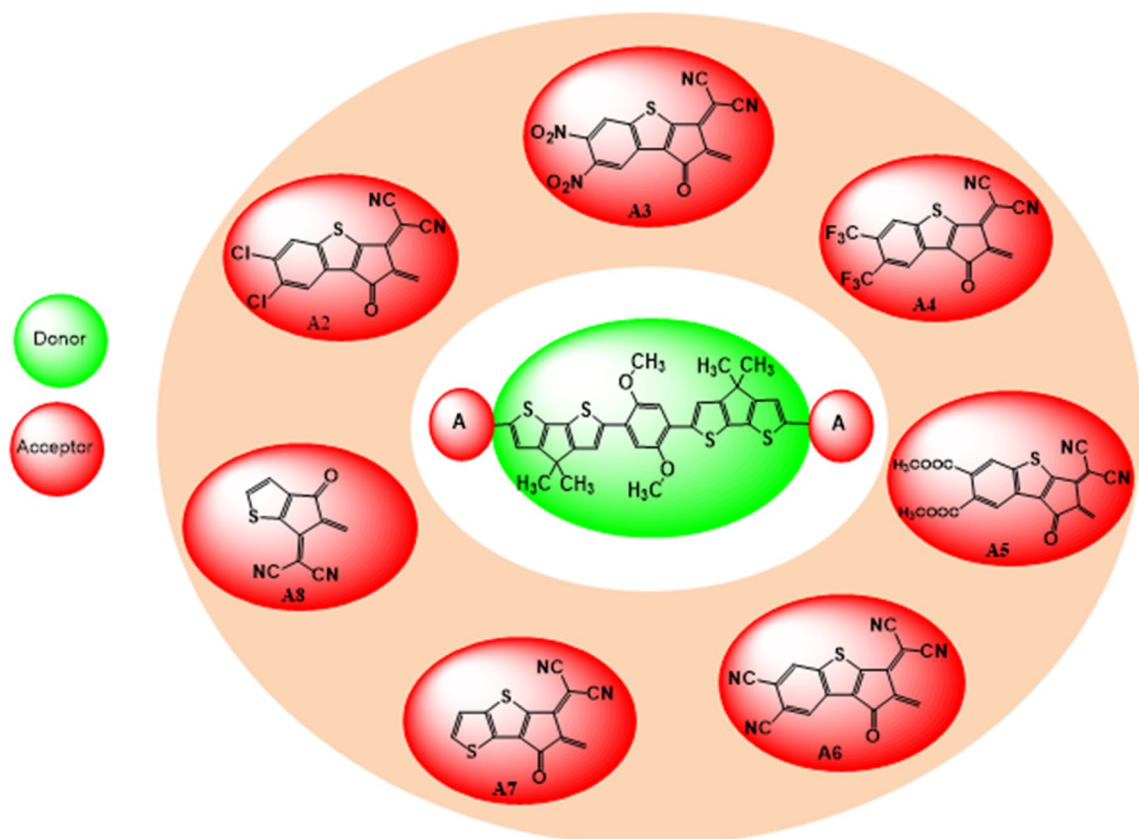


Figure 2. The sketch map of the reference and its derivative compounds.

in which the -Cl are altered with strong electron-withdrawing nitro (-NO₂) groups at the acceptor parts. This decline in band gap is due to the greater $-I$ effect of -NO₂ as compared to the -Cl groups (NO₂ > Cl). An increase in E_g (1.742 eV) is monitored in **MD4** in which the -NO₂ is exchanged with the trifluoromethyl (-CF₃) group. A slight enhancement in HOMO/LUMO band gap (1.779 eV) is expressed by **MD5** as compared to -CF₃ because of the exchange of -CF₃ with methyl acetate (-COOCH₃) at the acceptor units. This increase in E_g is accredited to the lower electron withdrawing ($-I$) effect of -COOCH₃ in comparison to the -CF₃ group. The $E_{\text{HOMO}}-E_{\text{LUMO}}$ band gap (1.628 eV) is noticed to be reduced in **MD6**. It is because of the higher $-I$ effect of -CN in comparison to -CF₃ and -COOCH₃. Also due to -CN, the charge transference rate is enhanced, resulting in lower E_g of orbitals. The highest E_g (1.988 eV) is found for **MD7** among all the designed molecules because of the removal of one fragment (phthalonitrile) of the acceptor moieties. Due to this reason the conjugation of the system is decreased as a result of which the band gap increased. E_g (1.940 eV) of **MD8** is retrieved to be less than the **MD7**, because of the incorporation of a thiophene ring at the peripheral acceptor units. As a result of which the conjugation in the molecule gets increased and the energy difference between the orbitals can be lowered. However, the overall descending trend of E_g is in the following order: **MD7** > **MR1** > **MD8** > **MD2** > **MD5** > **MD4** > **MD6** > **MD3**. Furthermore, scheme of electronic cloud on the surface area³⁵ of both **MR1** and **MD2**-**MD8** are represented in Fig. 4. Lowest E_g between the orbitals and efficient charge mobility from donor to end capped acceptors is inspected in **MD3** chromophore as compared to all other investigated chromophores which appeared to be an effective photovoltaic material.

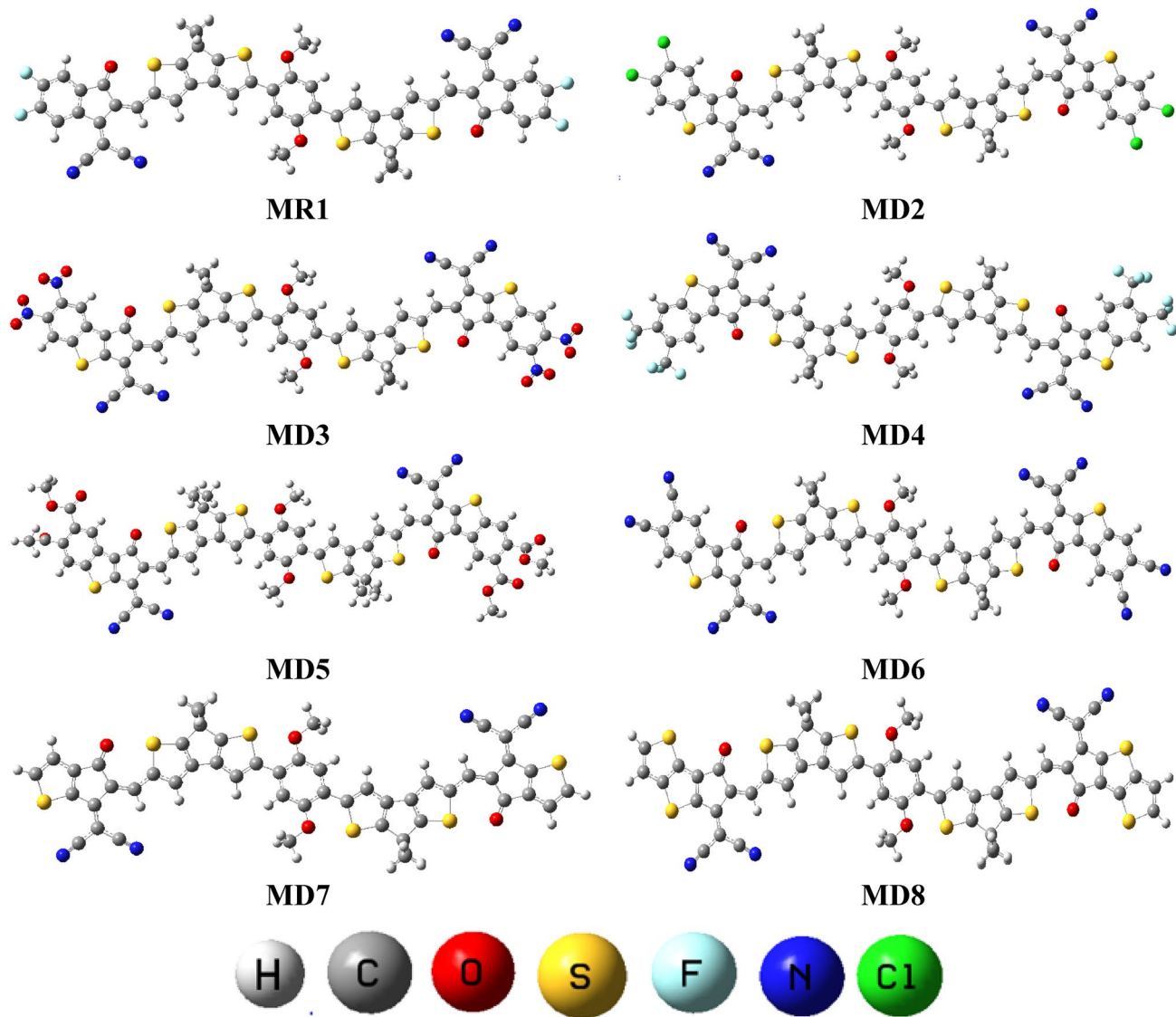


Figure 3. The optimized structures of all theoretically designed compounds. Figures are made with are made with the help of GaussView 5.0 and Gaussian 09 version D.01 (<https://gaussian.com/g09citation/>).

Compounds	E_{HOMO}	E_{LUMO}	E_{gap}
MR1	-5.176	-3.200	1.976
MD2	-5.158	-3.366	1.792
MD3	-5.217	-3.646	1.571
MD4	-5.180	-3.438	1.742
MD5	-5.161	-3.382	1.779
MD6	-5.210	-3.582	1.628
MD7	-5.125	-3.137	1.988
MD8	-5.116	-3.176	1.940

Table 1. Energy of frontier molecular orbitals and $E_{\text{LUMO}}-E_{\text{HOMO}}$ of MR1 and MD2–MD8. Units in eV.

Density of states (DOS). The DOS approach has been performed to determine the effective contribution of each fragment to all over the molecular system having specific number of electronic states³⁶. To predict the charge transfer path, we partitioned our compounds into two sections i.e., central donating core (D) and terminal acceptors (A). The DOS analysis of reference (MR1) and its derivatives was accomplished using B3LYP level of DFT with 6-31G(d,p) basis set to support FMO study (Fig. 4), DOS graphs are displayed in Fig. 5.

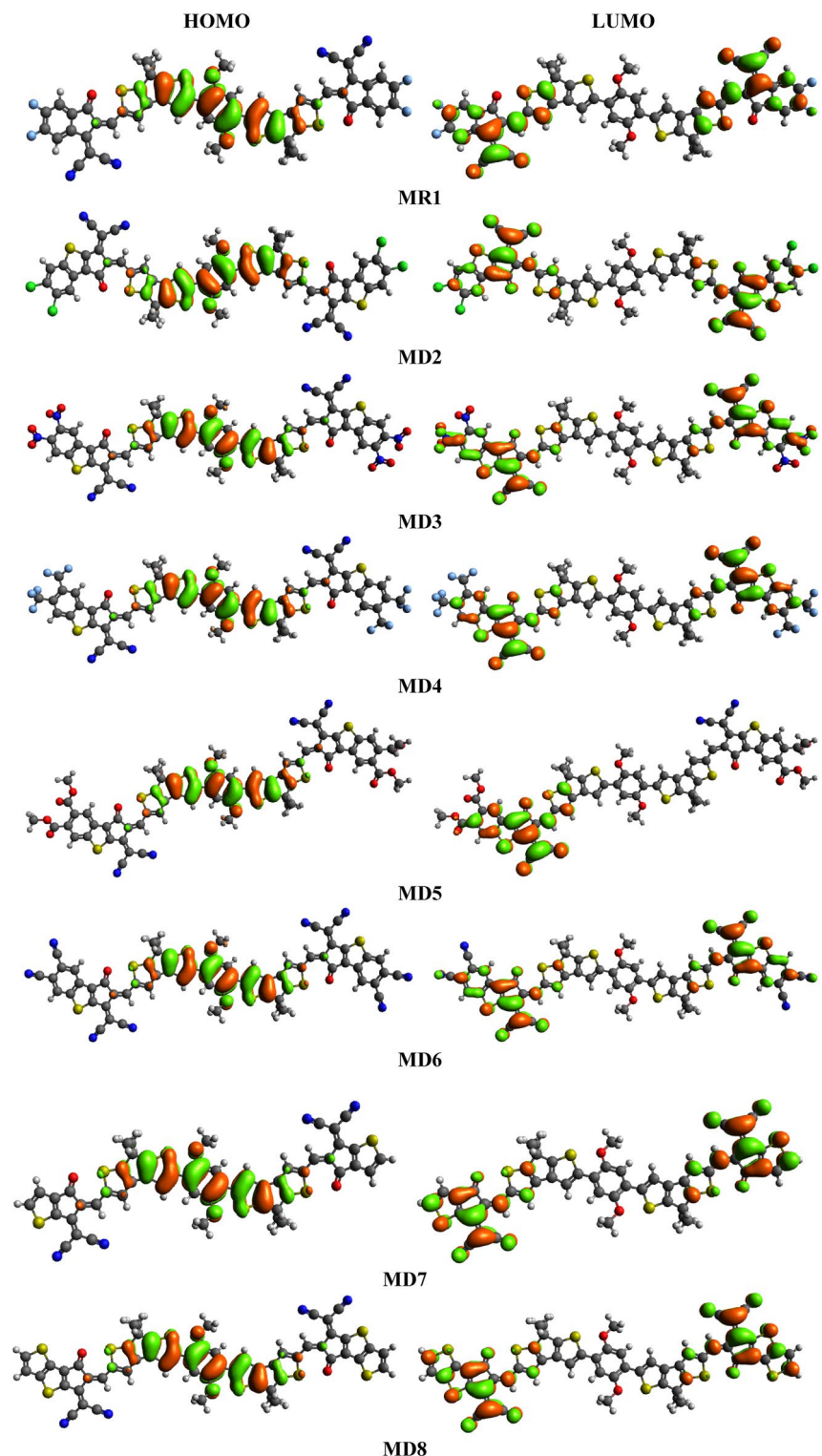


Figure 4. The FMOs (HOMOs & LUMOs) of the MR1 and MD2–MD8 drawn with the help of Avogadro software, Version 1.2.0. (<http://avogadro.cc/>). All out put files of entitled compounds were accomplished by Gaussian 09 version D.01 (<https://gaussian.com/g09citation/>).

As depicted in the Fig. 4 as well as manifested from Fig. 5 that electronic cloud is distributed around HOMO and LUMO because of strong electron pulling character of terminal acceptor groups. Similarly, to LUMO donor contributes 97.1, 97.2, 97.1, 97.1, 97.2, 97.2 and 97% to HOMO while 8.2, 7.6, 8.4, 8.2, 8, 11.5 and 8.4% to LUMO

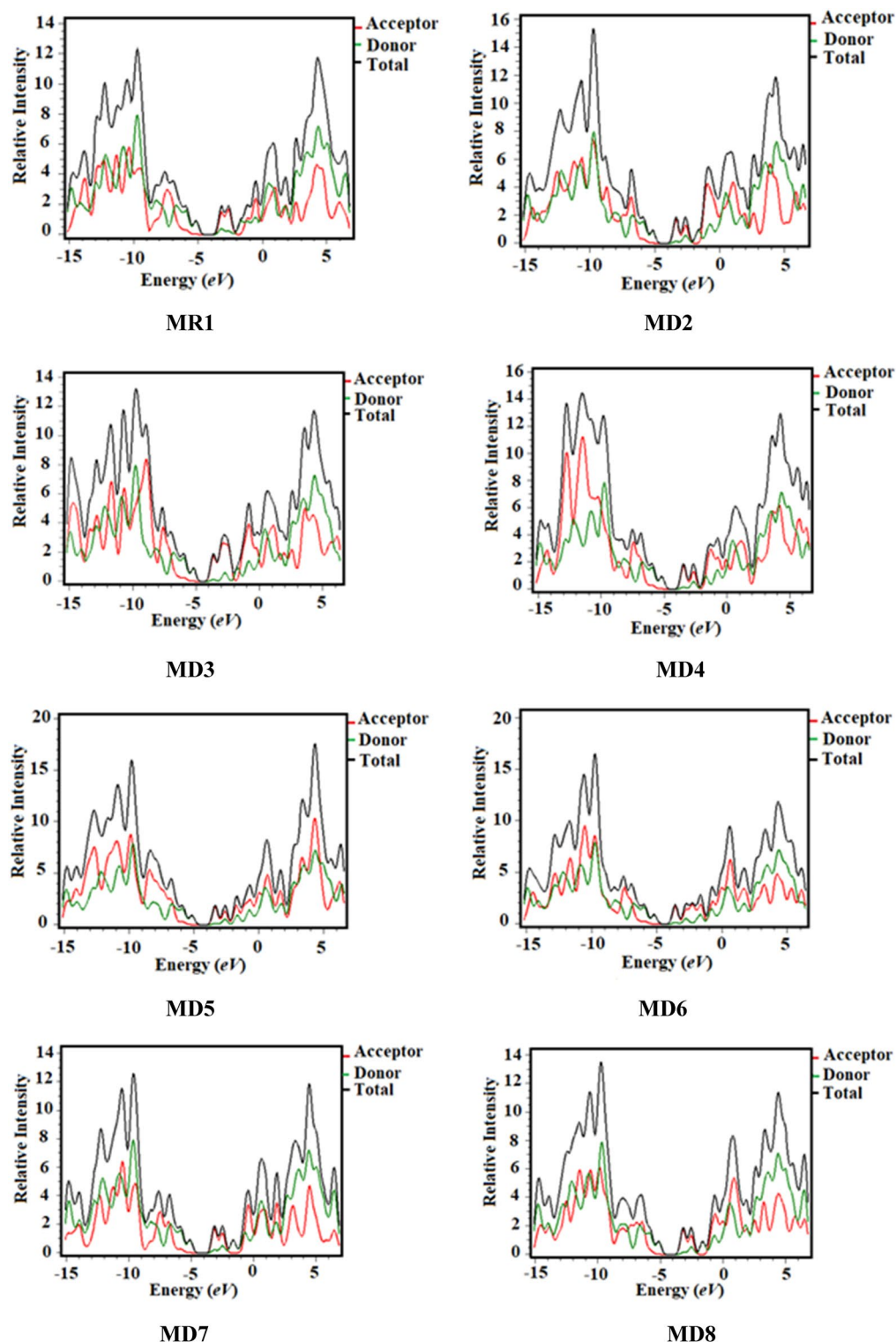


Figure 5. DOS spectra of the studied compounds (MR1 and MD2–MD8) drawn by utilizing PyMolyze 1.1 version (<https://sourceforge.net/projects/pymolyze/>). All out put files of entitled compounds were computed through Gaussian 09 version D.01 (<https://gaussian.com/g09citation/>).

in MD2–MD8, correspondingly. While acceptor contribution is 2.9, 2.8, 2.9, 2.9, 2.8, 2.8 and 3% to HOMO, while to LUMO 91.8, 92.4, 91.6, 91.8, 92, 88.5 and 91.6% for MD2–MD8, respectively. By these results, it is clear from DOS pictographs that the HOMO orbitals are positioned on the donating part shown with green colored peak

Compounds	λ (nm)	E (eV)	f_{os}	Assignments
MR1	738.221	1.680	0.250	H→L (98%)
MD2	814.186	1.523	0.132	H→L (98%)
MD3	939.844	1.319	0.134	H→L (99%)
MD4	840.742	1.475	0.130	H→L (98%)
MD5	819.893	1.512	0.115	H→L (89%)
MD6	906.649	1.368	0.131	H→L (99%)
MD7	725.690	1.709	0.158	H→L (98%)
MD8	744.158	1.666	0.141	H→L (97%)

Table 2. Calculated energies, wavelengths (λ_{\max}) and oscillation strengths for MR1 and MD2–MD8 in chloroform.

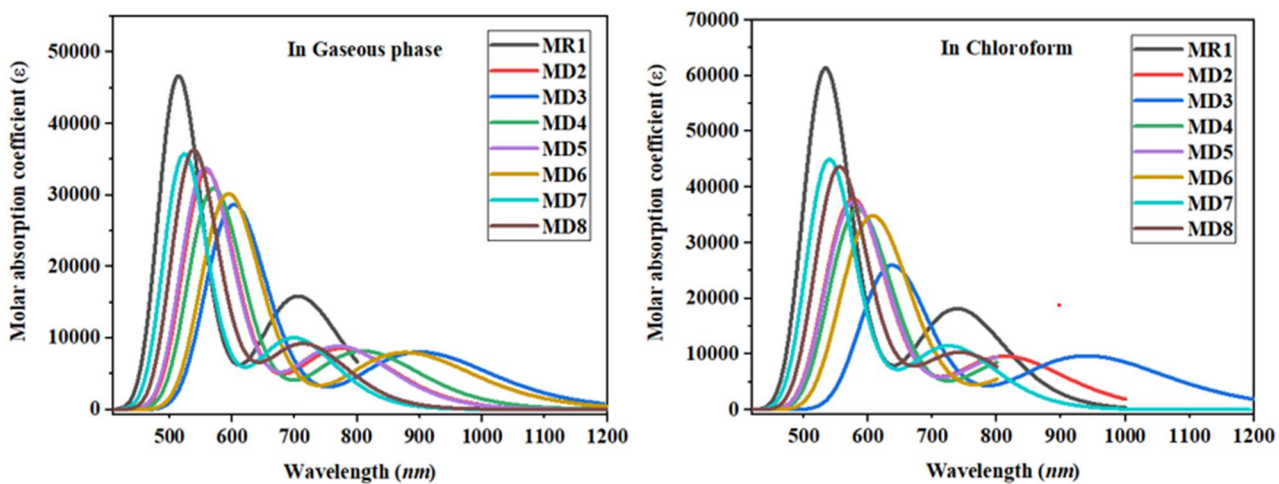


Figure 6. UV-visible absorption spectra of investigated molecules as their names can be seen in above graphs. These graphs are drawn by utilizing Origin Pro 8.5 version (<https://originpro.informer.com/8.5/>). All out put files of entitled compounds were computed through Gaussian 09 version D.01 (<https://gaussian.com/g09ciation/>).

which is found at -6.5 eV. Similarly, LUMOs are majorly resided on the acceptor moiety in aforesaid chromophores with higher peak at 1.5 eV. Overall, the separation pattern of charge distribution reveals that huge amount of charge is shifted in MD3 from donor towards acceptor moieties proving it to be most favorable candidate for non-fullerene OSCs applications.

Optical properties. To determine the effectiveness of OSCs, their optoelectronic capabilities are assessed by analyzing absorption spectra³⁷. To characterize their photophysical properties, absorption spectra of entitled chromophores (MR1 and MD2–MD8) were calculated in chloroform and gaseous phase at B3LYP/6-31G(d,p) level of theory. Numerous parameters like λ_{\max} , excitation energy, oscillator strengths (f) and molecular orbital contributions have been illustrated in Table 2 while UV-visible absorption spectrum of entitled molecules have been depicted in the Fig. 6. Generally strong electron accepting units leads to rise in the λ_{\max} with lower excitation energies than the reference MR1³⁸. This makes easy excitation between HOMO to LUMO causing higher charge transfer which ultimately lead to higher power conversion efficiency. The simulated λ_{\max} of reference chromophore in chloroform solvent (738.221 nm) shows good harmony with the experimental recorded λ_{\max} (743 nm)²⁷ of reference MR1 which also indicated the suitable selection of functional for DFT study.

The λ_{\max} ranges from 939.844 to 725.690 nm for entitled chromophores in chloroform. Among all designed molecules MD3 shows the maximum absorption wavelength of 939.844 nm that is attributed to highly electron accepting end capped Nitro group. Lower E_g and lower transition energies, both of these factors contribute to greater charge mobility and high-power conversion efficiency³⁸. Consequently, the lower value of λ_{\max} has been observed in the case of MD7 (725.690 nm) with excitation energy of 1.709 eV. All the explored chromophores possess higher absorption range than reference MR1 (738.221 nm) except MD7. It clear from Table 2 that MD2, MD4, MD5, MD6, and MD8 have maximum absorption values of 814.186, 840.742, 819.893, 906.649 and 744.158 nm respectively. Results indicate that λ_{\max} of all studied compounds lie in the visible region. Classification of entitled chromophores with respect to decreasing λ_{\max} in chloroform is MD3 > MD6 > MD4 > MD5 > MD2 > MD8 > MR1 > MD7.

Compounds	λ_{\max} (nm)	E (eV)	f_{os}	MO contributions
MR1	705.337	1.758	0.219	H \rightarrow L (99%)
MD2	776.162	1.597	0.118	H \rightarrow L (98%)
MD3	900.067	1.378	0.111	H \rightarrow L (99%)
MD4	808.927	1.533	0.113	H \rightarrow L (98%)
MD5	775.531	1.599	0.081	H \rightarrow L (96%)
MD6	877.081	1.414	0.110	H \rightarrow L (99%)
MD7	698.109	1.776	0.138	H \rightarrow L (98%)
MD8	713.742	1.737	0.127	H \rightarrow L (98%)

Table 3. Computed energy, wavelength (λ_{\max}) and oscillator strength for **MR1** and **MD2–MD8** in gaseous phase. HOMO = H, LUMO = L, f = oscillator strength, MO = molecular orbital.

Compounds	λ_e	λ_h
MR1	-0.001702	-0.004788
MD2	0.000152	-0.000132
MD3	0.000054	-0.000266
MD4	0.000133	-0.000264
MD5	0.000129	-0.000187
MD6	0.000123	-0.224763
MD7	0.000147	0.000025
MD8	0.000182	0.000029

Table 4. Computed reorganization energies of **MR1** and **MD2–MD8** chromophores.

In gaseous phase, all the investigated chromophores almost maintained the same order and properties as in chloroform. In gas phase, calculated λ_{\max} of all enlisted chromophores lies in the range of 900.067–698.109 nm. A small decrease in the values of λ_{\max} of entitled molecules in gas phase is noted which might be due to the solvent effect as shown in Table 3. In gas phase maximum absorbed wavelength decreases in the following order **MD3 > MD6 > MD4 > MD2 > MD5 > MD8 > MR1 > MD7**. The above trend concludes that **MD3** being the red shifted of all in absorption spectrum of both chloroform and gaseous phase would be an efficient OSC material.

Another crucial factor that can influence the electron mobility of entitled chromophores is excitation energy³⁹. Works concludes that molecule with small excitation energy hold improved charged mobilities, easy transition from valence to conduction band and higher PCE. The excitation energy values of all designed molecules are found less than the reference compound **MR1** except **MD7**. The lowest computed excitation energy of **MD3** is attributed to the strong electron pulling character of nitro group.

The preceding discussion concludes that all the designed molecules specifically **MD3** contain lower excitation energy and higher absorption thus having excellent potential to use in non-fullerene OSCs.

Reorganization energy. Reorganization energy (λ) is an imperative quantity in determining charge transfer characteristics among molecular structures while designing efficient materials for OSCs. The potential OSCs is mainly dependent upon the reorganization energy, which is actually the electron and hole transport ability of different materials. Generally, materials having good charge transport ability exhibit substantial optoelectronic properties⁴⁰. Reorganization energy and charge transfer capability have inverse relationship to each other, such that lower λ causes higher charge mobilities⁴¹. So, materials having higher charge mobilities ultimately have lower λ with widespread potential usage in non-fullerene OSCs. Reorganization energy varies with certain factors like nature of the molecule and their configuration but to a greater extent it is affected by geometries of cations and anions. Electron (λ_e) mobility has an association with anionic geometry while hole in acceptor material is represented by cationic geometry. Mainly, λ represents the charge transfer from donor to acceptor unit⁴². Overall, λ is categorized into two divisions; internal reorganization energy (λ_{int}) and external reorganization energy (λ_{ext}). The first one i.e. λ_{int} has founded its concerns with internal structural changes while λ_{ext} deals with the polarization influence. In this study, factor of external reorganization has not taken into consideration as external environment does not contribute much, so only λ_{int} is focused⁴³.

In this work, we theoretically calculated the reorganization energies of **MR1** and **MD2–MD8** utilizing Eqs. (1) and (2) and results are tabulated in Table 4.

From Table 4, it is clear that λ_e of reference compound **MR1** is -0.001702 eV. The computed electron mobilities of all entitled chromophores (**MD2–MD8**) are 0.000152, 0.000054, 0.000133 and 0.000129, 0.000123, 0.000147 and 0.000182 eV correspondingly. Reference compound **MR1** exhibit lower reorganization energy of electron (λ_e) indicating the higher electron transport abilities between donor and acceptor part. Among all the derivatives, **MD3** has the least value of λ_e which denotes the higher electron transport rate between HOMO

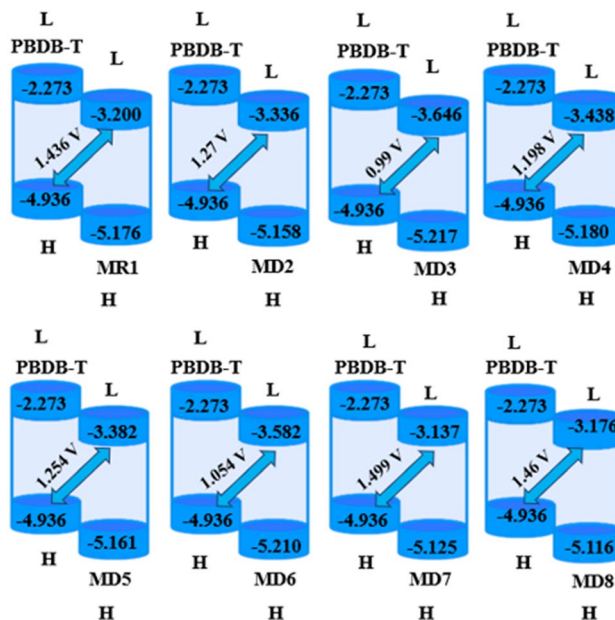


Figure 7. Diagrammatic illustration of V_{oc} for investigated molecules drawn with the aid of power point. All out put files of entitled compounds were accomplished by Gaussian 09 version D.01 (<https://gaussian.com/g09ciation/>).

and LUMO. Similarly, **MD6** and **MD5** considerably have better electron mobilities owing to their smaller value of λ_e . The λ_e values of all entitled chromophores decreases in the following order **MD8**>**MD2**>**MD7**>**MD4**>**MD5**>**MD6**>**MD3**>**MR1**.

Similarly, the theoretical calculated λ_h of **MR1** is -0.0004788 eV. The **MD2**–**MD8** show λ_h value of -0.000132 , -0.000266 , -0.000264 and -0.000187 , -0.224763 , 0.000025 and 0.000029 eV correspondingly. Among all, **MD3** is the finest molecule for hole transport capability owing to its smallest value of λ_h -0.000266 eV. The descending order of λ_h of all entitled chromophores is **MD6**>**MR1**>**MD7**>**MD4**>**MD5**>**MD2**>**MD8**>**MD3**.

The overall discussion concludes that, **MD3** is the molecule with best electron and hole transport abilities thus appeared to be the fine candidate to utilize in non-fullerene organic solar cell future applications.

Open circuit voltage (V_{oc}). Open circuit voltage being a vital parameter well indicates the performance and working mechanics of the semiconductor materials like OSCs⁴⁴. It represents the total magnitude of current that can be taken away from any optically active device at null voltage⁴⁵. Certain influential factors affecting the V_{oc} are; light source, light intensity, external fluorescence proficiency, recombination of charge carriers and various environmental features⁴⁶. To attain better V_{oc} , LUMO value of acceptor should be greater as compared to HOMO of donor moiety as it lowers band gap⁴⁷. Here in this manuscript, we related the results of LUMO of our tailored molecules with the HOMO of renowned polymer **PBDB-T**⁴⁸ having -4.936 eV as E_{HOMO} of donor polymer and results are summarized in Fig. 7. The computed V_{oc} results of **MR1** and **MD2**–**MD8** by means of Scharber equation⁴⁹ are tabulated in Table 5.

$$V_{oc} = (|E_{HOMO}^D| - |E_{LUMO}^A|) - 0.3 \quad (1)$$

Here, E is energy level, e indicates charge present on each molecule, and 0.3 is the empirical constant.

The V_{oc} value for **MR1** and **MD2**–**MD8** is 1.436, 1.27, 0.99, 1.198, 1.254, 1.054, 1.499 and 1.46 V respectively. A good harmony is seen between the simulated (0.85 V)²⁷ and experimental value (1.436 V) of reference chromophore which supports that suitable selection of functional for computational analysis. The computed V_{oc} value of compound **MD3** is 0.99 V. The V_{oc} of **MR1** with regards to $HOMO_{donor}$ – $LUMO_{MR1}$ is 1.436 V. **MD7** showed the highest V_{oc} (1.499 V). Except **MD7** and **MD8**, all the designed molecules showed lower values of V_{oc} than reference chromophore **MR1**. The decreasing order of V_{oc} of designed chromophores with respect to $HOMO_{donor}$ – $LUMO_{acceptor}$ is **MD7**>**MD8**>**MR1**>**MD2**>**MD5**>**MD4**>**MD6**>**MD3**. The band gap is an intrinsic property of semiconductors and eventually has a direct influence on the photovoltaic response of a compound. Band gap energy is the energy required for excitation from the highest occupied molecular orbital (HOMO) towards the lowest unoccupied molecular orbital (LUMO). Having low band gap means easy excitation or less energy will be required to excite electrons from HOMO to LUMO. If band gap is low, most photons will have more energy than necessary to excite electrons across the band gap generating more electricity with higher efficiency and large photovoltaic response. Herein, we reported our all-designed molecules which are of acceptor nature and are used in making bulk heterojunction devices by blended with polymer (PBDB-T) of donor type. When a complex of donor–acceptor formed we found that our all-designed chromophores have low energy of LUMO in comparison to LUMO of donor polymer. So, there will be a better transition from HOMO of

Compounds	ΔE (eV)	V_{oc} (V)
MR1	1.736	1.436
MD2	1.57	1.27
MD3	1.29	0.99
MD4	1.498	1.198
MD5	1.554	1.254
MD6	1.354	1.054
MD7	1.799	1.499
MD8	1.76	1.46

Table 5. V_{oc} of entitled molecules. $\Delta E = E_{\text{LUMO}}^{\text{A}} - E_{\text{HOMO}}^{\text{D}}$.

donor polymer to the low lying LUMO of our designed molecules in comparison to the LUMO of donor polymer with more knocking out of electrons and thus enhanced efficiencies. The orbital energy diagram with respect to **PBDB-T** of all molecules is shown in Fig. 6.

Transition density matrix (TDM) analysis. The interpretation of transition processes⁵⁰ and extent of intramolecular charge transfer within a conjugated system can be efficiently determined using transition density matrix (TDM). This analysis gives a pictorial display of interactions between donor and acceptor entities in excited state⁵¹ with three dimensional plots having sufficient color differentiation i.e., blue region displays⁵². In addition to this, the electron–hole localization and the extent of electronic movements in the specific regions of entitled chromophores (**MR1** and **MD2–MD8**) are indicated⁴¹. The behavior of transitions of entitled chromophores was investigated with B3LYP/6-31G(d,p) level of theory. In all the investigated compounds, the π -conjugation is absent and instead an A–D–A configuration is retained (Fig. 8). The H-atoms are neglected due to their minute influence in transitions as compared to the other atoms. The Fig. 8 represents the results obtained for TDM analysis for all the studied compounds.

To simplify the calculations in our present report, we categorized all structures (**MR1** and **MD2–MD8**) into two different areas i.e., donor (D) and acceptor (A). From TDM diagrams, it is evident that electron coherence is largely present on end capped acceptor portions as compared to donor entity. According to the results obtained from TDM heat maps, it has been observed that the electronic charge is efficiently transferred in diagonal way from the donor towards acceptor in all derivatives without trapping, showing a charge coherence. This makes clear that, donor and end-capped acceptor units efficiently donate and withdraw the electron density respectively. The most prominent charge shift is observed in compound **MD3**. This might be due to the presence of strong electron withdrawing nitro ($-\text{NO}_2$) group at acceptor units. Therefore, we can infer from the efficient charge transfer response that **MD3** chromophore could be conveniently utilized for the development of solar cell devices in the future⁵³.

Exciton binding energy (E_b) analysis. Another special feature related to TDMs is binding energy (E_b) that is used to assess the photovoltaic response of OSCs. It is an important parameter for the estimation of exciton dissociation capacity and columbic force interaction, as E_b declines, the columbic forces between hole and electron also decreases⁵⁴. Both these factors led to higher exciton dissociation in excited state^{55,56}. The E_b of investigated molecules **MR1** and **MD2–MD8** is calculated from the difference of E_{gap} (LUMO–HOMO) and energy of optimization (E_{opt})⁴³ as represented in the Eq. (2).

$$E_b = E_{\text{L-H}} - E_{\text{opt}} \quad (2)$$

In Eq. (2), E_b is binding energy, $E_{\text{L-H}}$ is the band gap between LUMO and HOMO and E_{opt} represents the first singlet to singlet excitation state energy⁵⁷. Calculated outcomes are tabulated in Table 6.

According to Table 6, **MD3** has given out lowest value of binding energy (0.252 eV) giving highest number of charges. In comparison to **MR1**, other molecules have smaller E_b providing reasonable justification for further calculations. Generally, structures with 1.9 eV or lower E_b are taken as efficient OSC materials with impressive V_{oc} . Interestingly, our all-investigated molecules possess E_b values smaller than 1.9 eV. The descending sequence of investigated chromophores related to E_b is as **MR1** > **MD7** > **MD8** > **MD2** > **MD4** > **MD5** > **MD6** > **MD3**. So, it is clear that among all investigated chromophores, **MD3** is the molecule with lowest value of E_b justifying greater magnitude of dissociation into free electrons with superior photo-electronic properties that describe it to be effective material for OSCs.

Conclusion

In this study, sophisticated quantum chemical procedures have utilized to examine photo-voltaic, photophysical and electronic capabilities of the explored derivatives. By performing structural modification in reference molecule (**MR1**) by end-capped acceptor moieties, seven new compounds (**MD2–MD8**) are designed. This terminal structural tailoring has proved to be the most important tactic to gain impressive photovoltaic compounds with improved opto-electronic possessions for efficient OSCs. Decrease in the energy gap of designed molecules (1.571–1.988 eV) is observed as compared with reference (1.976 eV) with efficient electron transfer rate

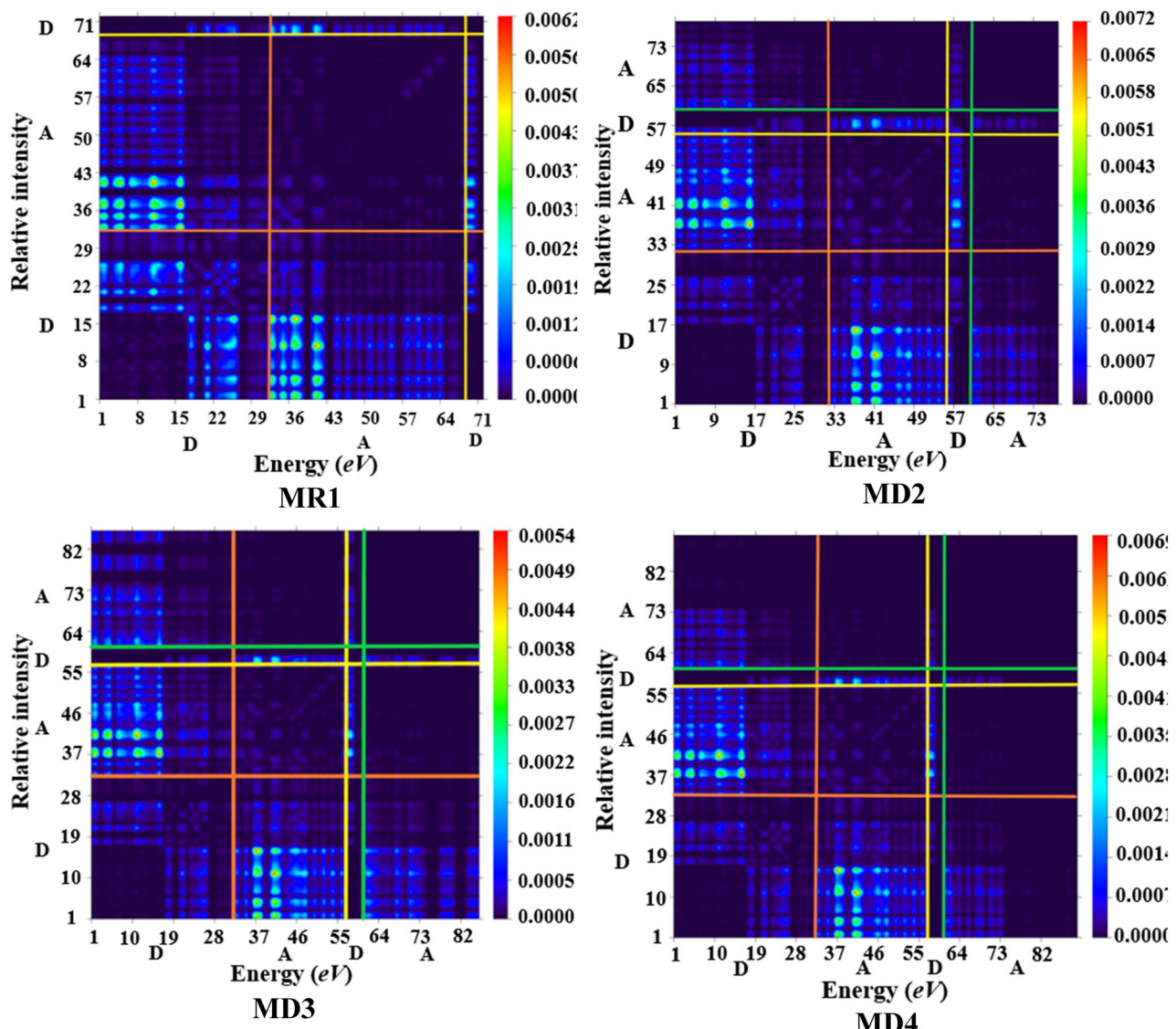


Figure 8. TDM for the entitled compounds (MR1 and MD2–MD8). These were drawn with the help of Multiwfn 3.7 software (<http://sobereva.com/multiwfn/>). All out put files of designed compounds were accomplished by Gaussian 09 version D.01 (<https://gaussian.com/g09citation/>).

from HOMO to LUMO, which is further, supported by DOS data. Further, the designed compounds exhibited a red shift in the visible region (939.844–725.690 nm) in chloroform solvent in comparison to reference **MR1** ($\lambda_{\max} = 738.221$ nm). Moreover, the V_{oc} is also estimated with regard to HOMO_{PBDB-T}–LUMO_{Acceptor}. Binding energy (E_b) of designed systems is smaller than **MR1** molecule, that elucidated the greater exciton dissociation rate, results in high-power conversion efficiency of fullerene free acceptor groups in OSCs.

Computational procedure

The entire theoretical calculations of the current work were computed employing the Gaussian 09⁵⁸ package. In order to visualize the designing of non-fullerene acceptor type chromophores and for the featuring of DFT based calculations, Gauss View 5.0⁵⁹ was utilized. TD-DFT calculations were carried out for the optimization of reference chromophore (**MR1**) by adapting different level of DFT such as B3LYP⁶⁰, CAM-B3LYP⁶¹, MPW1PW91⁶², M06⁶³, M06.2X⁶⁴ with 6-31G(d,p) basis set. Computed maximum absorbed wavelength of reference chromophore **MR1** at aforementioned functionals were compared with the experimental reported results for selecting valid theoretical method. λ_{\max} values of reference compound obtained using these functionals are 738.211, 439.380, 579.338, 565.028 and 446.436 nm correspondingly while experimental recorded λ_{\max} of parent chromophore, **DOC2C6-2F** is 743 nm²⁷. Functional B3LYP with 6-31G(d,p) had been shown the best agreement of DFT with experimental UV-visible results of **MR1** as displayed in Fig. 8 and was selected for computational analysis ahead.

Moreover, to visualize the effectiveness of enlisted chromophores, the electronic computations of the TDM, UV-Vis, E_b , V_{oc} , $E_{\text{HOMO}}-E_{\text{LUMO}}$ band gap analysis and reorganization energies are calculated employing the same B3LYP/6-31G(d,p) level of theory.

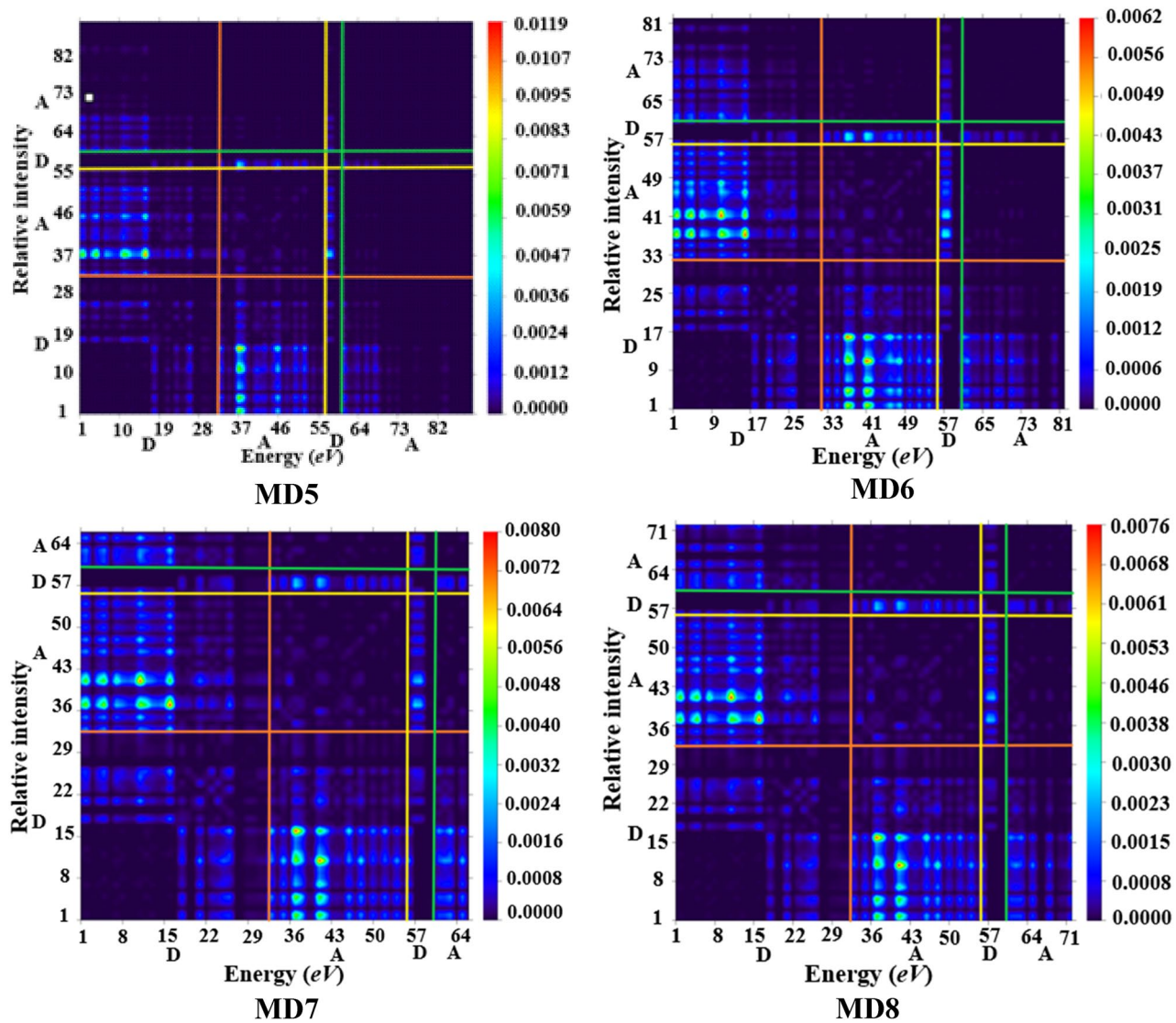


Figure 8. (continued)

Compounds	E_{L-H}	E_{opt}	E_b
MR1	1.976	1.680	0.296
MD2	1.792	1.523	0.269
MD3	1.571	1.319	0.252
MD4	1.742	1.475	0.267
MD5	1.779	1.512	0.267
MD6	1.628	1.368	0.260
MD7	1.988	1.709	0.279
MD8	1.940	1.666	0.274

Table 6. Calculated first singlet to singlet excitation state energy (E_{opt}) and binding energy (E_b) of inspected compounds. Units in eV.

Overall, λ is categorized into two main divisions. The first one i.e. internal reorganization has founded its concerns with internal structural variations while λ_{ext} deals with the polarization influence in the external environment. In this study, factor of external reorganization has not taken into consideration as external environment does not contribute much, so only λ_{int} is focused⁴³.

Hence, for the calculations of reorganization of electron (λ_e) and hole (λ_h) following Eqs. (3) and (4) are utilized.

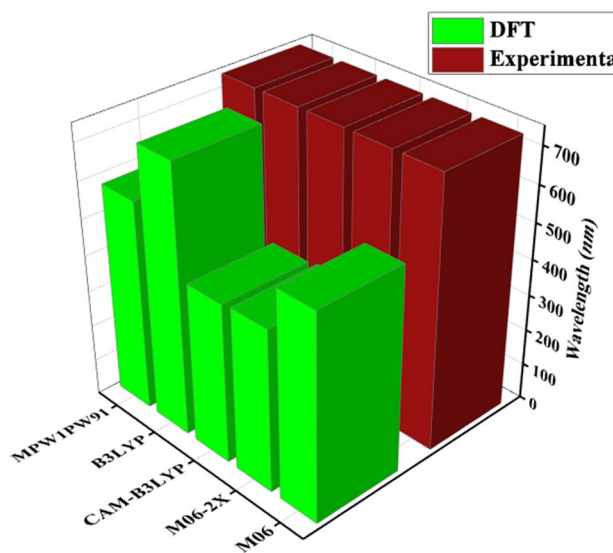


Figure 9. Comparison between DFT and experimental UV-visible results of **MR1** at various levels in chloroform solvent. These graphs are drawn by utilizing Origin Pro 8.5 version (<https://originpro.informer.com/8.5/>). All out put files of entitled compounds were computed through Gaussian 09 version D.01 (<https://gaussian.com/g09citation/>).

$$\lambda_e = [E_0^- - E_-] + [E_-^0 - E_0] \quad (3)$$

$$\lambda_h = [E_0^+ - E_+] + [E_+^0 - E_0] \quad (4)$$

While E_0^- and E_0^+ are the energies of neutral molecule via anion and cation optimized structures correspondingly, E_- and E_+ represents anionic and cationic energy, E_-^0 and E_+^0 are the energies of cationic and anionic structures via structures of neutral molecule (Fig. 9).

Data availability

All data generated or analyzed during this study are included in this published article and its supplementary information files.

Received: 9 June 2022; Accepted: 9 November 2022

Published online: 23 November 2022

References

1. Mao, J. *et al.* Graphene aerogels for efficient energy storage and conversion. *Energy Environ. Sci.* **11**, 772–799 (2018).
2. Doumon, N. Y. *et al.* Photostability of fullerene and non-fullerene polymer solar cells: The role of the acceptor. *ACS Appl. Mater. Interfaces*. **11**, 8310–8318 (2019).
3. Nian, L. *et al.* Ternary non-fullerene polymer solar cells with 13.51% efficiency and a record-high fill factor of 78.13%. *Energy Environ. Sci.* **11**, 3392–3399 (2018).
4. Lu, L. *et al.* Recent advances in bulk heterojunction polymer solar cells. *Chem. Rev.* **115**, 12666–12731 (2015).
5. Zhang, K. *et al.* Efficient large area organic solar cells processed by blade-coating with single-component green solvent. *Solar Rrl* **2**, 1700169 (2018).
6. Yao, H. *et al.* 14.7% efficiency organic photovoltaic cells enabled by active materials with a large electrostatic potential difference. *J. Am. Chem. Society*. **141**, 7743–7750 (2019).
7. Yu, G., Gao, J., Hummelen, J. C., Wudl, F. & Heeger, A. J. Polymer photovoltaic cells: Enhanced efficiencies via a network of internal donor-acceptor heterojunctions. *Science* **270**, 1789–1791 (1995).
8. Gao, J. *et al.* Over 16.7% efficiency of ternary organic photovoltaics by employing extra PC71BM as morphology regulator. *Sci. China Chem.* **63**, 83–91 (2020).
9. Mahmood, A. *et al.* A novel thiazole based acceptor for fullerene-free organic solar cells. *Dyes Pigm.* **149**, 470–474 (2018).
10. Khan, M. U. *et al.* Designing star-shaped subphthalocyanine-based acceptor materials with promising photovoltaic parameters for non-fullerene solar cells. *ACS Omega* **5**, 23039–23052 (2020).
11. Luo, Z. *et al.* Altering the positions of chlorine and bromine substitution on the end group enables high-performance acceptor and efficient organic solar cells. *Adv. Energy Mater.* **10**, 2002649 (2020).
12. Khan, M. U. *et al.* Novel W-shaped oxygen heterocycle-fused fluorene-based non-fullerene acceptors: First theoretical framework for designing environment-friendly organic solar cells. *Energy Fuels* **35**, 12436–12450 (2021).
13. Adnan, M. *et al.* Fine tuning the optoelectronic properties of triphenylamine based donor molecules for organic solar cells. *Z. Phys. Chem.* **231**, 1127–1139 (2017).
14. Liu, J. *et al.* Fast charge separation in a non-fullerene organic solar cell with a small driving force. *Nat. Energy* **1**, 1–7 (2016).
15. Zhan, X. *et al.* A high-mobility electron-transport polymer with broad absorption and its use in field-effect transistors and all-polymer solar cells. *J. Am. Chem. Soc.* **129**, 7246–7247 (2007).
16. Lin, Y. & Wang, J. Z.-. G. Zhang, H. Bai, Y. Li, D. Zhu, X. Zhan. *Adv. Mater* **27**, 1170 (2015).

17. Mahmood, A., Tang, A., Wang, X. & Zhou, E. First-principles theoretical designing of planar non-fullerene small molecular acceptors for organic solar cells: Manipulation of noncovalent interactions. *Phys. Chem. Chem. Phys.* **21**, 2128–2139 (2019).
18. Jia, J. *et al.* The effect of end-capping groups in ADA type non-fullerene acceptors on device performance of organic solar cells. *Sci. China Chem.* **60**, 1458–1467 (2017).
19. Wang, J. *et al.* Enhancing performance of nonfullerene acceptors via side-chain conjugation strategy. *Adv. Mater.* **29**, 1702125 (2017).
20. Kan, B. *et al.* A chlorinated low-bandgap small-molecule acceptor for organic solar cells with 14.1% efficiency and low energy loss. *Sci. China Chem.* **61**, 1307–1313 (2018).
21. Lin, Y. *et al.* An electron acceptor challenging fullerenes for efficient polymer solar cells. *Adv. Mater.* **27**, 1170–1174 (2015).
22. Fei, Z. *et al.* An alkylated indacenodithieno [3, 2-b] thiophene-based nonfullerene acceptor with high crystallinity exhibiting single junction solar cell efficiencies greater than 13% with low voltage losses. *Adv. Mater.* **30**, 1705209 (2018).
23. Cheng, P., Li, G., Zhan, X. & Yang, Y. Next-generation organic photovoltaics based on non-fullerene acceptors. *Nat. Photonics* **12**, 131–142 (2018).
24. Yuan, J. *et al.* Single-junction organic solar cell with over 15% efficiency using fused-ring acceptor with electron-deficient core. *Joule* **3**, 1140–1151 (2019).
25. Liang, N., Jiang, W., Hou, J. & Wang, Z. New developments in non-fullerene small molecule acceptors for polymer solar cells. *Mater. Chem. Front.* **1**, 1291–1303 (2017).
26. Wang, R. *et al.* Rational tuning of molecular interaction and energy level alignment enables high-performance organic photovoltaics. *Adv. Mater.* **31**, 1904215 (2019).
27. Huang, H. *et al.* Noncovalently fused-ring electron acceptors with near-infrared absorption for high-performance organic solar cells. *Nat. Commun.* **10**, 1–10 (2019).
28. Khan, M. U. *et al.* Designing triazatruxene-based donor materials with promising photovoltaic parameters for organic solar cells. *RSC Adv.* **9**, 26402–26418 (2019).
29. Janjua, M. R. S. A. *et al.* Effect of π -conjugation spacer (CC) on the first hyperpolarizabilities of polymeric chain containing polyoxometalate cluster as a side-chain pendant: A DFT study. *Comput. Theor. Chem.* **994**, 34–40 (2012).
30. Khan, M. U. *et al.* Prediction of second-order nonlinear optical properties of D- π -A compounds containing novel fluorene derivatives: A promising route to giant hyperpolarizabilities. *J. Cluster Sci.* **30**, 415–430 (2019).
31. Khan, M. U. *et al.* Quantum chemical designing of indolo [3, 2, 1-jk] carbazole-based dyes for highly efficient nonlinear optical properties. *Chem. Phys. Lett.* **719**, 59–66 (2019).
32. Adnan, M., Mehboob, M. Y., Hussain, R. & Irshad, Z. In silico designing of efficient C-shape non-fullerene acceptor molecules having quinoid structure with remarkable photovoltaic properties for high-performance organic solar cells. *Optik* **241**, 166839 (2021).
33. Khalid, M., Imran, M., Braga, A. A. C. & Akram, M. S. Molecular engineering of indenoindene-3-ethylrodanine acceptors with A2-A1-D-A1-A2 architecture for promising fullerene-free organic solar cells. *Sci. Rep.* **11**, 1–15 (2021).
34. Khalid, M., Lodhi, H. M., Khan, M. U. & Imran, M. Structural parameter-modulated nonlinear optical amplitude of acceptor- π -D- π -donor-configured pyrene derivatives: A DFT approach. *RSC Adv.* **11**, 14237–14250 (2021).
35. Khalid, M. *et al.* First principles study of electronic and nonlinear optical properties of A-D- π -A and D-A-D- π -A configured compounds containing novel quinoline-carbazole derivatives. *RSC Adv.* **10**, 22273–22283 (2020).
36. Adeel, M. *et al.* Exploration of CH- \cdots F & CF- \cdots H mediated supramolecular arrangements into fluorinated terphenyls and theoretical prediction of their third-order nonlinear optical response. *RSC Adv.* **11**, 7766–7778 (2021).
37. Khan, M. U. *et al.* First theoretical framework of triphenylamine-dicyanovinylene-based nonlinear optical dyes: Structural modification of π -linkers. *J. Phys. Chem. C* **122**, 4009–4018 (2018).
38. Ans, M., Iqbal, J., Eliasson, B. & Ayub, K. Opto-electronic properties of non-fullerene fused-undecacyclic electron acceptors for organic solar cells. *Comput. Mater. Sci.* **159**, 150–159 (2019).
39. Raza, A. R. *et al.* A facile microwave assisted synthesis and structure elucidation of (3R)-3-alkyl-4, 1-benzoxazepine-2, 5-diones by crystallographic, spectroscopic and DFT studies. *Spectrochim. Acta Part A Mol. Biomol. Spectrosc.* **230**, 117995 (2020).
40. Khalid, A. *et al.* Designing benzothiadiazole based non-fullerene acceptors with high open circuit voltage and higher LUMO level to increase the efficiency of organic solar cells. *Optik* **228**, 166138 (2021).
41. Ans, M. *et al.* Designing three-dimensional (3D) non-fullerene small molecule acceptors with efficient photovoltaic parameters. *ChemistrySelect* **3**, 12797–12804 (2018).
42. Khan, M. U. *et al.* Designing spirobifullerene core based three-dimensional cross shape acceptor materials with promising photovoltaic properties for high-efficiency organic solar cells. *Int. J. Quantum Chem.* **120**, e26377 (2020).
43. Hussain, R. *et al.* Molecular engineering of A-D-C-D-A configured small molecular acceptors (SMAs) with promising photovoltaic properties for high-efficiency fullerene-free organic solar cells. *Opt. Quant. Electron.* **52**, 1–20 (2020).
44. Irfan, M. *et al.* Design of donor-acceptor-donor (D-A-D) type small molecule donor materials with efficient photovoltaic parameters. *Int. J. Quantum Chem.* **117**, e25363 (2017).
45. Tang, S. & Zhang, J. Design of donors with broad absorption regions and suitable frontier molecular orbitals to match typical acceptors via substitution on oligo (thienylenevinylene) toward solar cells. *J. Comput. Chem.* **33**, 1353–1363 (2012).
46. Saleem, R., Farhat, A., Khera, R. A., Langer, P. & Iqbal, J. Designing of small molecule non-fullerene acceptors with cyanobenzene core for photovoltaic application. *Comput. Theor. Chem.* **1197**, 113154 (2021).
47. Bai, H. *et al.* Acceptor-donor-acceptor small molecules based on indacenodithiophene for efficient organic solar cells. *ACS Appl. Mater. Interfaces* **6**, 8426–8433 (2014).
48. Zheng, Z. *et al.* PBDB-T and its derivatives: A family of polymer donors enables over 17% efficiency in organic photovoltaics. *Mater. Today* **35**, 115–130 (2020).
49. Scharber, M. C. *et al.* Design rules for donors in bulk-heterojunction solar cells—Towards 10% energy-conversion efficiency. *Adv. Mater.* **18**, 789–794 (2006).
50. Ans, M., Ayub, K., Bhatti, I. A. & Iqbal, J. Designing indacenodithiophene based non-fullerene acceptors with a donor-acceptor combined bridge for organic solar cells. *RSC Adv.* **9**, 3605–3617 (2019).
51. Gangala, S. K., Paramasivam, M., Dyaga, B. & Rao, V. J. Energy levels tuning of 'Z'-shaped small molecular non-fullerene electron acceptors based on dipyrrrolo [2, 3-b; 2', 3'-e] pyrazine-2, 6 (1H, 5H)-dione acceptor unit for organic photovoltaic applications: a joint experimental and DFT investigation on the effect of fluorination. *New J. Chem.* (2019).
52. Arshad, M. N., Shafiq, I., Khalid, M. & Asiri, A. M. Exploration of the intriguing photovoltaic behavior for fused indacenodithiophene-based A-D-A conjugated systems: A DFT model study. *ACS Omega* **7**, 11606–11617 (2022).
53. Hussain, R. *et al.* Enhancement in photovoltaic properties of N, N-diethylaniline based donor materials by bridging core modifications for efficient solar cells. *ChemistrySelect* **5**, 5022–5034 (2020).
54. Khalid, M. *et al.* Enriching NLO efficacy via designing non-fullerene molecules with the modification of acceptor moieties into ICIF2F: An emerging theoretical approach. *RSC Adv.* **12**, 13412–13427 (2022).
55. Dkhissi, A. Excitons in organic semiconductors. *Synth. Met.* **161**, 1441–1443 (2011).
56. Farhat, A., Khera, R. A., Iqbal, S. & Iqbal, J. Tuning the optoelectronic properties of Subphthalocyanine (SubPc) derivatives for photovoltaic applications. *Opt. Mater.* **107**, 110154 (2020).

57. Köse, M. E. Evaluation of acceptor strength in thiophene coupled donor–acceptor chromophores for optimal design of organic photovoltaic materials. *J. Phys. Chem. A* **116**, 12503–12509 (2012).
58. Frisch, M. J. & Clemente, F. R. Gaussian 09, revision a. 01, mj frisch, gw trucks, hb schlegel, ge scuseria, ma robb, jr cheeseman, g. Scalmani, V. Barone, B. Mennucci, GA Petersson, H. Nakatsuji, M. Caricato, X. Li, HP Hratchian, AF Izmaylov, J. Bloino, G. Zhe 20–44 (2009).
59. Gandomi, F., Vakili, M., Darugar, V., Takjoo, R. & Tayyari, S. F. Optimized molecular geometry, vibrational analysis, and Fe–O bond strength of Tris (α -cyanoacetylacetone) iron (III): An experimental and theoretical study. *J. Mol. Struct.* **1248**, 131444 (2022).
60. Civalleri, B., Zicovich-Wilson, C. M., Valenzano, L. & Ugliengo, P. B3LYP augmented with an empirical dispersion term (B3LYP-D*) as applied to molecular crystals. *CrystEngComm* **10**, 405–410 (2008).
61. Yanai, T., Tew, D. P. & Handy, N. C. A new hybrid exchange–correlation functional using the Coulomb-attenuating method (CAM-B3LYP). *Chem. Phys. Lett.* **393**, 51–57 (2004).
62. Adamo, C. & Barone, V. Exchange functionals with improved long-range behavior and adiabatic connection methods without adjustable parameters: The m PW and m PW1PW models. *J. Chem. Phys.* **108**, 664–675 (1998).
63. Bryantsev, V. S., Diallo, M. S., Van Duin, A. C. & Goddard, W. A. III. Evaluation of B3LYP, X3LYP, and M06-class density functionals for predicting the binding energies of neutral, protonated, and deprotonated water clusters. *J. Chem. Theory Comput.* **5**, 1016–1026 (2009).
64. Zhao, Y. & Truhlar, D. G. The M06 suite of density functionals for main group thermochemistry, thermochemical kinetics, noncovalent interactions, excited states, and transition elements: two new functionals and systematic testing of four M06-class functionals and 12 other functionals. *Theoret. Chem. Acc.* **120**, 215–241 (2008).

Acknowledgements

Dr. Muhammad Khalid gratefully acknowledges the financial support of HEC Pakistan (project no. 20-14703/NRPU/R&D/HEC/2021). Authors are also thankful for cooperation and collaboration of A.A.C.B from IQ-USP, Brazil especially for his continuous support and providing computational lab facilities. M.A. expresses appreciation to the Deanship of Scientific Research at King Khalid University Saudi Arabia through the research groups program under grant number R.G.P.2/83/43.

Author contributions

M.K.: Methodology; software; supervision. R.A.: Data curation; formal analysis. I.S.: Conceptualization; methodology; software. M.A.: Data curation; formal analysis. M.A.A.: Resources; software. M.I.: Conceptualization; resources, supervision. A.A.C.B.: Data curation; formal analysis; validation. K.S.M.: Conceptualization; methodology.

Competing interests

The authors declare no competing interests.

Additional information

Supplementary Information The online version contains supplementary material available at <https://doi.org/10.1038/s41598-022-24087-8>.

Correspondence and requests for materials should be addressed to M.K.

Reprints and permissions information is available at www.nature.com/reprints.

Publisher's note Springer Nature remains neutral with regard to jurisdictional claims in published maps and institutional affiliations.



Open Access This article is licensed under a Creative Commons Attribution 4.0 International License, which permits use, sharing, adaptation, distribution and reproduction in any medium or format, as long as you give appropriate credit to the original author(s) and the source, provide a link to the Creative Commons licence, and indicate if changes were made. The images or other third party material in this article are included in the article's Creative Commons licence, unless indicated otherwise in a credit line to the material. If material is not included in the article's Creative Commons licence and your intended use is not permitted by statutory regulation or exceeds the permitted use, you will need to obtain permission directly from the copyright holder. To view a copy of this licence, visit <http://creativecommons.org/licenses/by/4.0/>.

© The Author(s) 2022